A Physical Model for Drying of Gelcast Ceramics*

Sarbajit Ghosal, Abbas Emami-Naeini
SC Solutions, Santa Clara, CA 95054

Ywh-Pyng Harn
Octant Technologies Inc., Santa Clara, CA 94086

Barry S. Draskovich, John P. Pollinger
AlliedSignal Ceramic Components, Torrance, CA 90504

Abstract

Gelcasting is a promising new technology for manufacturing advanced structural ceramic components. The process involves drying of the 'green' gelcast part before densification. The physical mechanisms controlling this relatively long drying process are not well understood. In this study, several controlled experiments were performed to elucidate the key mechanisms. A one-dimensional drying model was formulated based on evaporation and gaseous diffusion through the part. Experimental data were used to obtain correlations for model parameters. This model predicts the instantaneous moisture content of a gelcast sample with an accuracy of better than 10% when dryer humidity and temperature, and sample thickness are specified.

Keywords: gelcasting, ceramic, drying, process, model.

1 Introduction

Gelcasting is a relatively new method for fabricating the powder compacts used in manufacturing advanced structural ceramic parts such as turbine components for the aerospace and other industries [1, 2, 3, 4]. The gelcasting process involves preparation of an aqueous slurry of sub-micron ceramic particles (e.g., alumina or silicon nitride) together with small quantities of gel initiators, catalysts, monomers, cross-linkers, and sintering aids.

Gelation is initiated after the slurry is poured into a simple or complex shaped mold and the temperature elevated. The macromolecular network resulting from this *in situ* polymerization holds the ceramic particles together. After removal from the mold, the gelled part contains about a quarter of its mass as moisture which is then removed by drying. The part is then heated to burn out the polymer gel, and subsequently gas pressure-sintered for densification. The final product is a near-net shaped part that requires very little machining. Other advantages of gelcasting over traditional ceramic forming processes include faster casting and a less expensive densification process [1, 4].

Drying of pure gels is a complex, multiphase transport process. A survey of the current state of sol-gel and ceramic sciences shows that while several qualitative or semi-quantitative studies of gel drying [5, 6] and ceramic drying [7, 8] are available in the literature, there are no validated global process models, i.e., models that predict gel drying rates

*This work is partially funded by the Defense Advanced Research Projects Agency (DARPA, Cooperative Agreement Number N00014-95-2-0006) and administered by the Office of Naval Research (ONR). Funding balance and program execution is provided by the Advanced Structural Ceramics Virtual Company (ASCVC), led by AlliedSignal, Inc.

when ambient temperature and humidity are specified. However, these studies have successfully identified the physical mechanisms for moisture transport during different stages of drying in gels and gelcast parts.

In this paper, we propose a physical model for gelcast drying that uses experimental data to estimate key model parameters. Of the various mechanisms involved, only the mechanism which limits the overall rate of moisture removal from the part at any stage of the drying process is considered in the model.

A study of the experimental data obtained by drying a silicon nitride (Si_3N_4) gelcast part in a commercial dryer shows three distinguishable regions in the drying profile. Figure 1 shows these three stages for a typical drying process, the mass of the sample being measured every two minutes. Since the set contains over five hundred data points, only the line joining these points is shown. The second graph shows the calculated drying rate which is rather 'noisy'. The drying stages can be better distinguished in the third graph where the rate data were smoothed using a first-order lowpass Butterworth filter with a cut-off frequency of 0.5 Hz. The drying rate remains constant at about 9 g/hr for the first hour of drying, and then decreases steadily for the next nine hours, and finally flattens out at about 0.5 g/hr.

Three stages have also been noted in the drying of pure gels [6], and we have used terminology commonly used for gel drying. There is a constant rate drying period (CRP) in the initial part of the drying cycle which is relatively short. In this stage, which is referred to here as Stage 1 drying, there is also a linear shrinkage of 3–4% of the gelcast part. The shrinkage, measured with a contact dimension sensor, decreases with increased solids loading of the slurry, and is much smaller than the linear shrinkage of $\approx$50% experienced when drying pure gels [6].

The constant rate drying period is followed by a non-linear drying rate period when the drying rate decreases with time. This falling rate period (FRP) is referred to here as drying Stage 2. There is very little change in sample dimensions in this stage. The final drying profile in Stage 3 is approximately linear with a small slope, i.e., with a low drying rate. The experiments showed that the switching points between the stages on the drying curve depends on the drying conditions (temperature and relative humidity) and sample thickness. The next section describes the drying process in more detail.

The current empirically-guided drying process for parts which are about an inch thick can take several days, and is the longest stage in the gelcast manufacturing process. Hence, the drying stage can become a bottleneck in a manufacturing environment. Consequently, it is necessary to design an optimal drying cycle whereby the drying period is minimized without causing any damage to the part. This physical model was used in designing and implementing a model-based feedback controller for optimal drying which is described elsewhere [9].

2 Physical Mechanism of Gelcast Drying

The drying mechanism proposed here is now described using a simplified schematic shown in Figure 2. The Si_3N_4 ceramic particles in the gelcast part are uniformly distributed throughout the polymer gel with little physical contact between particles. These particles have a nominal size of 0.5 μm, and are equiaxed. These particles constitute approximately half of the gelcast part volume and about three-quarters of the total mass. In Stage 1 drying, the moisture, in the form of liquid water, is transported primarily by capillary forces to the part surface where it evaporates to the atmosphere at a constant rate. The gel matrix yields to the large compressive stresses set up by the capillary forces. The Si_3N_4 particles, firmly attached to the polymer network, move towards each other when the network collapses, which in turn causes a bulk shrinkage of the part. The part shrinks at about the same (volume) rate as the water evaporation rate, causing the water level to be maintained at the sample surface. Once all the particles touch each other, further movement among them ceases. At this point, the moisture begins to recede from the part surface. In thicker samples,

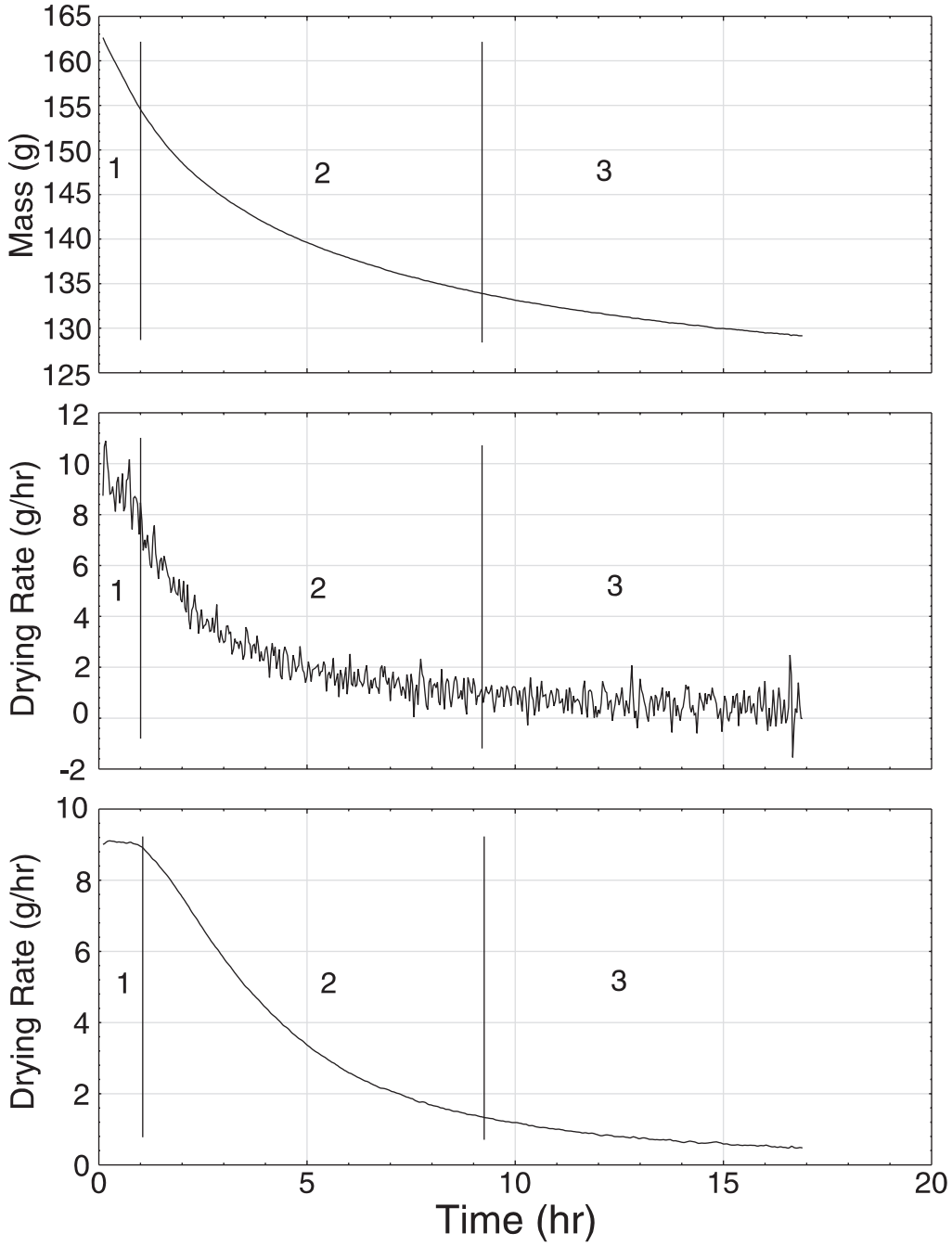

Figure 1: Drying profile for a gelcast part showing the three stages of drying. The dryer temperature was 40°C and relative humidity was 45%. The sample diameter and thickness were 3.1 cm and 2.5 cm, respectively. The top graph shows the dynamic sample mass measured during drying. The graph in the middle shows the drying rate calculated using the mass measurements. The bottom graph is the result of filtering the drying rates shown in the second graph to reduce 'noise'.

however, particles may continue to rearrange without significant dimensional changes.

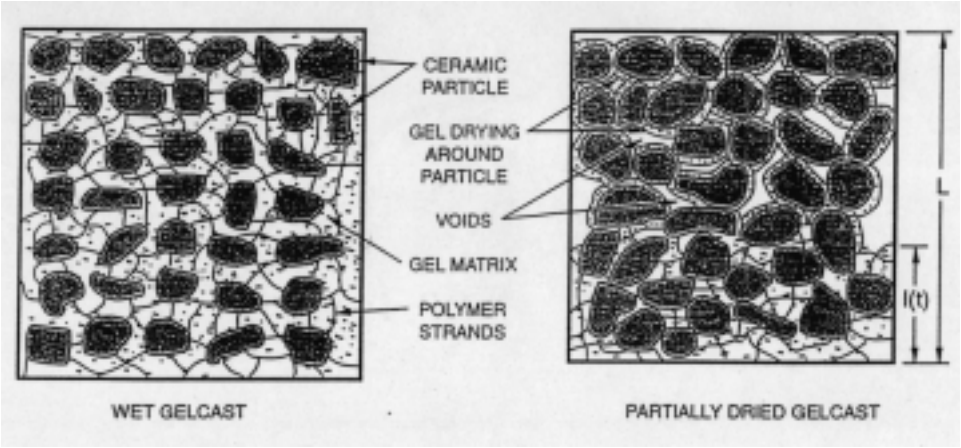

Figure 2: Magnified schematic representation of a microscopic cross-section of a drying gelcast part. Although the polymer chains criss-cross the entire inter-particle space, only a few are shown here to retain clarity, the rest being denoted by the shaded gel matrix. Apart from moist air, the inter-particle voids in the partially dried part also contains dried gel polymer that are not shown.

As the part continues to dry, the gel which coats the individual Si_3N_4 particles begins to shrink while remaining attached to the particles. In the process of this shrinkage towards particle surfaces, the gel-matrix ruptures[*]. As shown in Figure 2, this rupturing gives rise to interconnected 'voids', which may be empty spaces but are more likely to contain 'strands' of polymer gel. However, these interparticle spaces are comparable to the size of the particles, and significantly larger than the 'pores' *within* the gel matrix[†].

While the gel shrinks around individual particles, moisture in the gel matrix is transported to the surface of the gel-coated particles primarily by capillary forces. On reaching the particle surfaces, the moisture (or 'free' water) is initially transported to the part surface by capillary forces even without further shrinkage of the part.[‡] Thus, Stage 1 drying may continue beyond the shrinkage stage. However, the capillary forces transporting the water through the voids is smaller than the capillary forces in the gel pores because of the large size of voids. Hence, the water level cannot be sustained near the part surface, and beyond some point in the drying cycle, it recedes deeper into the part.

The 'free' water now evaporates into the inter-particle voids, marking the start of FRP or Stage 2 drying. Once the partial pressure of water vapor in the voids reaches saturation vapor pressure, the water vapor must be removed from the part before further evaporation can take place. However, this 'free' water seeps out to the particle surfaces faster than the water vapor diffusion through the porous gelcast part. Hence, the latter process is rate limiting in drying at this stage. Furthermore, this 'free' water forms continuous or isolated pockets which have the effect of disconnecting the water vapor pockets (present deeper in the part) from the gaseous path to the part surface, thus preventing moisture transport. The part has to dry away from the surfaces and towards the center. As a result, the water vapor diffuses through increasingly longer pore lengths, and hence driven by decreasing concentration gradients. Consequently, the mass loss rate decreases with time.

Once the polymer gel stops shrinking around individual gel-coated particles in the gelcast part, capillary forces are soon insufficient to transport water to the particle surfaces. As the gel coat around the particles dry up, it is likely that

[*] Note that this gel tearing does not cause macroscopic cracking or warping of the sample.

[†] These nanometer-sized pores are spaces between the polymer chains that constitute the gel network.

[‡] This phenomenon is called capillary penetration or infiltration [10].

the porous networks collapse. The remaining moisture (≈5–20% of the total) then reaches the inter-particle voids *via* diffusion through the dense, dried polymer layer. This diffusion process, however, is much slower than diffusion of water vapor through the porous gelcast part, and hence is rate-limiting. This Stage 3 drying rate is much slower than those in the first two stages.

3 Drying Experiments

The experiments performed in this study showed, as expected, that lower humidities and higher temperatures create higher drying potentials (and higher drying rates), while relatively higher humidities and lower temperatures create lower drying potential. Thicker samples correspond to longer transport distances and, hence, result in drying rates that are much smaller than those for thin gelcast parts. Three sets of drying experiments were conducted on disc shaped silicon nitride gelcast samples, each with a diameter of 10 cm. In each set, one of the parameters (i.e., humidity, temperature or thickness) was varied in each experiment while the other two were kept constant for all experiments in that set. These experiments revealed the relative sensitivity of drying rates to ambient (dryer) humidity and temperature, and sample thickness, and helped determine model parameters. The sample was dried in an aluminum mold that was open at one surface, forcing the sample to dry only from one of its two flat faces. The moisture movement was thus restricted to one (vertical) dimension, with negligible evaporation from the circumferential surface.

Commercial grade silicon nitride powder, consisting of nominally monodisperse equiaxed particles of size 0.5 μm, was used for producing the gelcast specimens. The gelation system used to form the test samples was developed at ORNL and is described in detail elsewhere [1, 2, 3]. It consists of a monomer – Methacrylamide, and a crosslinker – N,N+- Methylenebisacrylamide, as the major constituents, accompanied by small amounts of initiator and catalyst added to support the thermally activated free-radical polymerization reaction. The silicon nitride test specimen gel systems used in this study contained 4.5% weight of gel precursors (based on dry weight of ceramic powder). When gelled, the test specimens consisted of 51.2% gel by volume, before drying.

A commercial dryer[¶] was used for gelcast drying. The dryer's temperature and humidity sensors are RTD (resistance temperature device) and capacitative devices, respectively. The air within the dryer chamber was mixed *via* continuous recirculation. Experiments on the dryer indicated that its response times for temperature and humidity ramps used in the drying cycle were significantly shorter than the time scales for gelcast drying.

An electronic weight balance[§] was used as the mass sensor, along with RS232 interface for sending data to the data acquisition and control unit [9]. The balance was located outside and below the dryer chamber, thus protected from the heat and humidity fluctuations in the chamber. The platform supporting the sample was mounted on a rod which, in turn, was mounted on the balance pan through a small opening in the chamber floor.

The four experiments in the first set (Set 1) were conducted at 40°C, 50°C, 70°C, and 80°C, respectively. The relative humidity was 45% and the sample was 1.0 cm thick. Three experiments in Set 2 were performed at relative humidities of 75%, 30%, and 15% on a sample of thickness 1.0 cm. The dryer temperature was held at 50°C. Experiments in the final set (Set 3) were carried out at 45% relative humidity and 50°C temperature on samples with thicknesses of 0.3 cm, 0.5 cm, 1.0 cm, and 1.7 cm. In all the experiments, the temperature and humidity remained constant during the drying cycle. This range of temperatures, humidities, and thicknesses span the range of interest for current gelcast parts and drying conditions. Apart from experiments in these three sets, a few others were done under

[¶] Tenney© model Versatenn 2.
[§] Mettler©, model RM400.

different drying conditions for cross-validation of the model.

The experimental results served four purposes. First, the data were used to determine the points on the drying curve where the model switches from one stage to the next in various drying conditions. Second, the data were used to determine the temperature dependence of saturation vapor pressure of water in the gel. Third, the data were used to calculate an effective diffusivity of water vapor through the network of voids in the part. Finally, the effective diffusion coefficient of water vapor through the dried polymer coat around particles was obtained from the data. These issues are discussed further in the next section.

4 Gelcast Drying Model

The one-dimensional (1–D) drying model described here assumes an overall uni-directional moisture movement. The cylindrical disc geometry that served as the experimental sample is used in describing the physical model. The sample dries in the mold from one horizontal face whose area is A (in m^2). The sample thickness is L (in m), and the moisture gradients are in the vertical direction[‡].

4.1 Stage 1 Drying: Constant Rate Period

In Stage 1, the moisture is at or very close to the surface, and the drying *via* evaporation is similar to water evaporating from a pan. An analysis of this moisture transport is available in the literature, e.g., Holman [11] and Cussler [12]. The expression for the constant (i.e., time-independent) evaporation (drying) rate, derived from Fick's law of diffusion, is shown below:

$$\dot{m}_1 = DACM_w \frac{\mathrm{d}y}{\mathrm{d}z} \tag{1}$$

Here, $\dot{m}_1$ is the rate of evaporative mass loss (units: kg/s), D is diffusivity of water vapor in air (m^2/s), M_w is the molecular weight of water vapor (18 kg per kg-mole), and C is the total molar concentration (moles/m^3) in air which, in turn, is obtained from the ideal gas equation:

$$C = \frac{P}{R_o T}$$

P is the pressure (atmospheric pressure of 101325 Pa in this case), R_o is the Universal Gas Constant (8314 J/kg-mole.K), and T the absolute temperature in K. The term $\frac{\mathrm{d}y}{\mathrm{d}z}$ denotes the gradient of the mole fraction of water vapor in the direction normal to the surface (units: 1/m). This gradient depends strongly on the ambient relative humidity and the presence (or absence) of convective flow. We can approximate the term as a linear concentration profile (boundary layer):

$$\frac{\mathrm{d}y}{\mathrm{d}z} = \frac{y_{sat} - y_Z}{Z} = \frac{y_{sat} \cdot (1 - RH)}{Z}$$

Here, the saturation mole fraction, y_{sat} is given by $y_{sat} = p_{sat}/P$, and the mole fraction, y_Z at a distance Z is obtained from the relative humidity, RH, using $y_Z = RH \cdot y_{sat}$. The length, Z, is a measure of the concentration boundary layer thickness. It is measured experimentally in the case of evaporation of water from rivers and seas for various conditions such as wind speeds and temperatures [11]. From our experiments we find Z for this dryer to be 5.4 mm. The circulated air with controlled humidity enters the chamber about 30 cm above the sample surface, resulting in a somewhat smaller concentration gradient (and larger value of Z) than that achieved by blowing the air directly over the sample surface.

[‡]Had the part dried uniformly from both faces, L would be equal to half of the part thickness.

Diffusivity of a gas increases with temperature and decreases with pressure. An explanation of this dependence is given by Bird, *et al* [13]. The final form of the relationship for diffusivity, D, of water vapor (units: m^2/s) is found to be:

$$D = \frac{2.527}{P} \cdot \left(\frac{T}{292.86}\right)^{2.334} \tag{2}$$

The saturation vapor pressure of water, p_{sat} (3.1 kPa at 22°C), is a strong function of temperature, and increases rapidly with temperature to atmospheric pressure at the boiling point. For water associated with the gel (including water at the sample surface), p_{sat} is expected to be lower compared with water drying from a pan, as predicted from thermodynamic considerations by the Gibbs-Thompson (or Kelvin) equation [5]. In the model, p_{sat} was calculated as a best-fit parameter. A quadratic polynomial in temperature, T (in K), was fit to these p_{sat} values (in Pa) obtained from drying data at four temperatures (Set 1 experiments). The polynomial is:

$$p_{sat} = 3.08\,T^2 - 1829.5\,T + 277257$$

These values of p_{sat} are lower, and the temperature dependence of p_{sat} is less steep, when compared with water drying from a pan. It is noted that this correlation is restricted to gelcast parts drying in the temperature range of 40°C–80°C.

A non-dimensional drying rate for Stage 1, m'_1, is obtained by normalizing $\dot{m}_1$ against the total moisture content of the sample, m_o, where $m_o = \rho\ (f\,A\,L)$. Here, ρ is the density of water, and f is the volume fraction of water in the sample (0.488 in this study). After integrating Equation 1, we obtain the dynamic moisture content of the sample at time t in Stage 1 to be:

$$m'(t) = \frac{m_o - \int_0^t \dot{m}_1\,\mathrm{d}t}{m_o} = 1 - \left[\frac{D M_w\, p_{sat}\ (1 - RH)}{\rho\, L\, R_o\, T\, Z}\right] t \tag{3}$$

Here, $m'(t)$ decreases from unity to close to zero at the end of Stage 3. Stage 1 drying concludes at $t = t_1$ with a moisture fraction of X_1, where $X_1 = m'(t_1)$.

4.2 Stage 2 Drying: Falling Rate Period

In Stage 2 (FRP), the moisture diffuses through the network of voids in the gelcast part. Here, the Fickian diffusion transport process is enhanced by a bulk (advective) movement of moisture-laden air out of the part [11] so that the rate of change of moisture mass is:

$$\dot{m}_2 = -\frac{D_e A_e C M_w}{z} \ln\left(\frac{1 - y_L}{1 - y_{sat}}\right) \tag{4}$$

Here, D_e is the diffusivity of the water vapor through the porous gelcast part. The moisture gradient is in the vertical z direction, and the vapor path length z, which increases with time, is taken to be $(L - l(t))$. Here, $l(t)$ is the height of the 'free' water as shown in Figure 2. The area, A_e, is the total area of contact of the 'free' water with air. Evaporation occurs over this area which is estimated from the volume fraction to be $A_e \equiv 0.94\,f\,A$. The coefficient 0.94 accounts for a 6% decrease in the surface area following shrinkage. As in CRP, $y_L = y_{sat} \cdot RH$, and the moisture concentration profile is given by [12]:

$$\frac{1 - y(z)}{1 - y_{sat}} = \left(\frac{1 - y_L}{1 - y_{sat}}\right)^{z/L}$$

The dynamic moisture mass is related to $l(t)$ as

$$\dot{m}_2(t) = \rho A_e \dot{l}(t) \tag{5}$$

The effect of the concentration gradient of air in the pore on moisture transport is expected to be very small for this relatively dilute gas mixture of water vapor in air, and is neglected. After substitutions for $\dot{m}_2$ and y_L, Equation 4 takes the following non-linear form.

$$\dot{l}(t) \;=\; -\,\frac{D_e C M_w}{\rho\,(L - l(t))}\,\ln\left(\frac{1 - RH.y_{sat}}{1 - y_{sat}}\right) \tag{6}$$

The normalized rate is obtained by dividing both sides of Equation 6 by L. The equation is then integrated to obtain the dynamic moisture content, $m'(t)$, of Stage 2:

$$m'(t) \;=\; 1 - \int_{t_1}^{t} \frac{\dot{l}(t)}{L}\,\mathrm{d}t \;=\; 1 - \left[(1 - X_1)^2 \;+\; \left\{\frac{2 D_e C M_w}{\rho L^2}\,\ln\left(\frac{1 - RH.y_{sat}}{1 - y_{sat}}\right)\right\}\,(t - t_1)\right]^{1/2} \tag{7}$$

Thus, we see that the moisture in the part decreases non-linearly during Stage 2. Stage 2 drying concludes at $t = t_2$ with a moisture fraction of X_2, where $X_2 = m'(t_2)$.

The effective diffusivity of water vapor through the voids, D_e, is defined as $D_e \;=\; K_D\,.\,D$. The following relationship was used to relate the correction factor, K_D, ($K_D \leq 1$) to the gelcast part thickness, L (in m) in the thickness range of 0.3 mm–17 mm:

$$K_D \;=\; 1 - 1.62\exp(-269.29\,L)$$

The effective diffusivity appears to increase with sample size, which may have to do with the location of the point at which evaporation occurs within the sample. During drying this point retreats to a depth where the rate of evaporation matches the rate of capillary flow (in the liquid film along particle surfaces) from the interior. As the sample thickness increases, it may be possible to drain a larger fraction of the water by capillary flow to the drying front. In such a case, the front recedes more and more slowly into the sample so that evaporation occurs at (nearly) a fixed distance from the exterior. Consequently, the diffusion path length does not scale with L, the sample size which, in turn, makes D_e seem to increase with L.

4.3 Stage 3 Drying: Polymer Diffusion Period

The Stage 3 model calculates the moisture retained in each gelcast particle and the particle surface area (assuming spherical particles). Using a best-fit effective diffusivity, the model calculates a moisture flux out of each particle using Fick's law to model water vapor diffusion through the dense polymer, assuming that the gel-coated particle dries uniformly inwards from the gel surface towards the particle surface. Since polymer diffusion is the rate-limiting process, the net moisture flux out of the gelcast part is calculated by multiplying the flux out of each particle by the total number of particles. The result is a closed-form expression for a constant-rate drying model. Clearly, there are several major simplifications in the model such as identical, independently-drying particles characterized by a single effective diffusivity.

The (radially uniform) molar flux of water vapor through the gel coat of each particle, $\dot{n}$, is given by Fick's law [12] as

$$\dot{n} \;=\; -\,D_p\,(4\pi r_o^2)\,\frac{\mathrm{d}c}{\mathrm{d}r} \tag{8}$$

Here, D_p, is the effective diffusivity of water molecules through the drying (or dried) polymer gel (in m^2/s), c is the molar concentration of water in the gel (in moles/m^3), r_o is the radius of a spherical gel-coated particle (in m), and r is the radial position, $r_s \leq r \leq r_o$, where r_s is the radius of the uncoated particle. The effective relative humidity, RH', inside the gel is arbitrary chosen as the average of saturation relative humidity (i.e., unity) and the dryer relative humidity, i.e.,

$$RH' \;=\; \frac{1 + RH}{2}$$

Assuming a constant molar gradient across the gel coat, we have:

$$\frac{\mathrm{d}c}{\mathrm{d}r} \;=\; -C\left(\frac{y_{sat}-y_{RH'}}{r_o-r_s}\right)$$

Here, y_{sat} and $y_{RH'}$ are the moisture mole fractions at saturation and effective relative humidity, respectively. Since $y_{RH'} = RH'.y_{sat}$, and $C = P/(R_o T)$ we get:

$$\frac{\mathrm{d}c}{\mathrm{d}r} \;=\; -\frac{P y_{sat}\,(1-RH')}{R_o T\,(r_o-r_s)} \tag{9}$$

The total number of particles in the sample, N_p, is given by:

$$N_p \;=\; \frac{(1-f)\,V}{\frac{4}{3}\pi r_s^3}$$

Here, V is the gelcast sample volume. Substituting the expression for molar gradient from Equation 9 into Equation 8, and multiplying the result by N_p and M_w, one obtains the following expression for the *total* diffusive mass flux, $\dot{m}_3$ (units: kg/s), out of the gelcast part:

$$\dot{m}_3 \;=\; 3\,(1-f)\,V C y_{sat} M_w\,(1-RH')\left(\frac{\gamma^2}{\gamma-1}\right)\frac{D_p}{r_s^2} \tag{10}$$

Here, $\gamma = r_o/r_s = 1.23$ for particles distributed uniformly in a gelcast part with a volume fraction of 0.488. The particle radius, r_s, is 0.25 μm.

The effective diffusivity, D_p, was calculated by fitting Equation 10 to the data. The following relatively simple temperature dependence yielded a reasonably good fit, and is similar to the correlation used for D_e in Stage 2 (T in K, D_p in m^2/s).

$$D_p \;=\; 5\times 10^{-17}\left(\frac{T}{300}\right)^2$$

Such small values of D_p is reasonable, since it is known that diffusivity is anomalously low for polar molecules such as water, because of interaction with the polymer molecules [5].

The moisture loss rate in Equation 10 is normalized by the total moisture mass at the beginning of Stage 3, and then integrated to yield the non-dimensional moisture content of the part in Stage 3:

$$m_3(t) \;=\; X_2 \;-\; K\,.\,(t-t2) \tag{11}$$

Here,

$$K \;=\; \frac{3\,(1-f)\,(1-RH')\,V C y_{sat} M_w}{X_2\,.\,m_o}\cdot\frac{\gamma^2}{\gamma-1}\cdot\frac{D_p}{r_s^2}$$

The experiments indicated that a small fraction of the moisture remains trapped in the sample even under conditions of high drying potential. The minimum value of the residual moisture was ≈2%. For this reason, the drying period is considered to have ended after 98% of the moisture has been removed.

Expressions for mass transfer coefficients, h, (units: m/s) which are conventionally used in drying models, can be obtained by dividing the evaporation rates ($\dot{m}_1, \dot{m}_2$, or $\dot{m}_3$) by the product of the sample surface area and the difference in mass concentrations. For Stages 2 and 3, these coefficients decrease with time and are not very physically meaningful. However, for Stage 1, the mass transfer coefficient for this dryer is easily calculated, and it increases with increasing operating temperatures:

$$h_1 \;=\; \frac{\dot{m}_1}{(M_w C\Delta y)\,A} \;=\; \frac{\dot{m}_1}{M_w C y_{sat}\,(1-RH)\,A} \;=\; \frac{D}{Z}$$

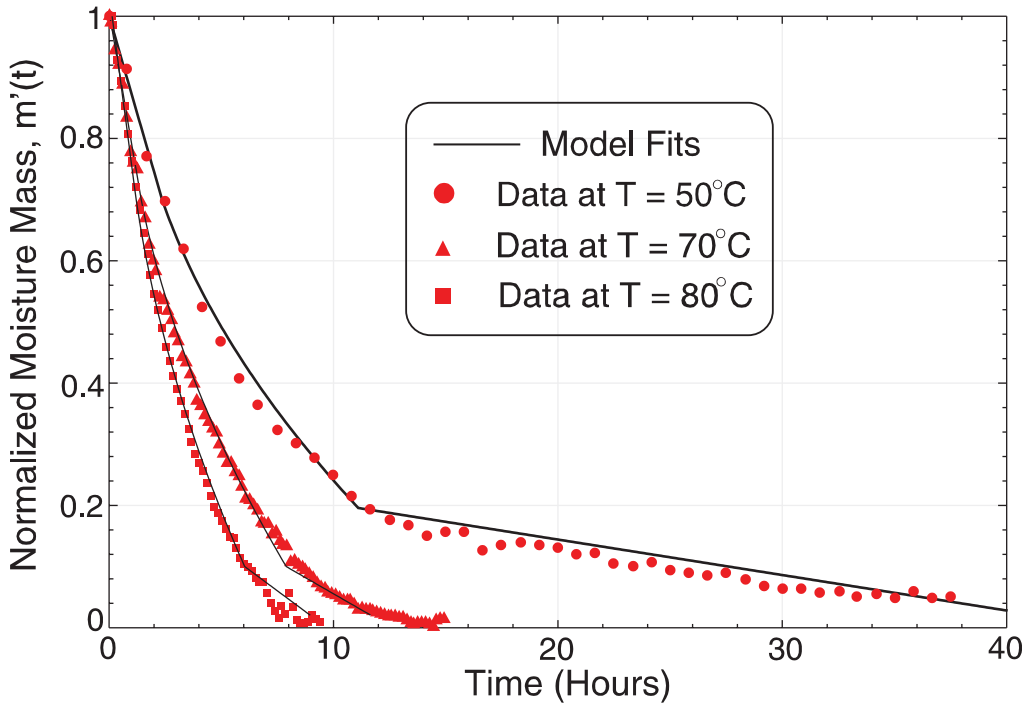

Figure 3: Drying profile for dryer temperatures of 50°C, 70°C, and 80°C. The dryer relative humidity was 45%, and the sample diameter and thickness were 10 cm and 1 cm, respectively. The solid lines show the drying model fits to the data.

5 Results and Discussion

Drying model correlation to the data are shown next in a series of figures. The ordinate shows the non-dimensional moisture mass, $m'(t)$, at time t (in hours). For some experiments, actual drying began some time after the data acquisition clock had started to record time. The moisture mass at start of drying is 24.4% of the sample mass, and is used in calculating $m'(t)$. Figures 3 and 4 show the effect of temperature and relative humidity on the drying profiles, respectively (experiments in Set 1 and Set 2). Finally, Figure 5 shows the drying profiles of gelcast samples of varying thickness at 50°C and 45% humidity (Set 3 experiments).

It is evident from the data that, in contrast to this idealized 1–D model, there is no distinct transition point from Stage 2 to Stage 3. The reason is that as the 'free' water level recedes into the part, Stage 3 drying commences for the gel-coated ceramic particles closer to the surface. This simultaneous occurrence of Stage 2 and Stage 3 drying effectively smooths out the drying profile.

It is noted that the initial linear drying regime tends to last longer for lower drying potentials (i.e, with larger RH and smaller T), and larger sample thickness, L. At higher drying potentials and smaller L, the rate of capillary penetration is smaller than the evaporation rate, and the water level recedes into the part rather quickly. Additionally, the effect of Stage 3 is significantly reduced at higher temperatures and smaller sample thicknesses.

Figure 6 shows two cases of model validation, where the model was used to predict drying rates at different drying conditions. Comparison with the data is quite good. For the sample of thickness 0.3 cm drying at 40°C and a relative humidity of 45%, the average and maximum difference in $m'(t)$ between model and data were 1.6% and 5.2%,

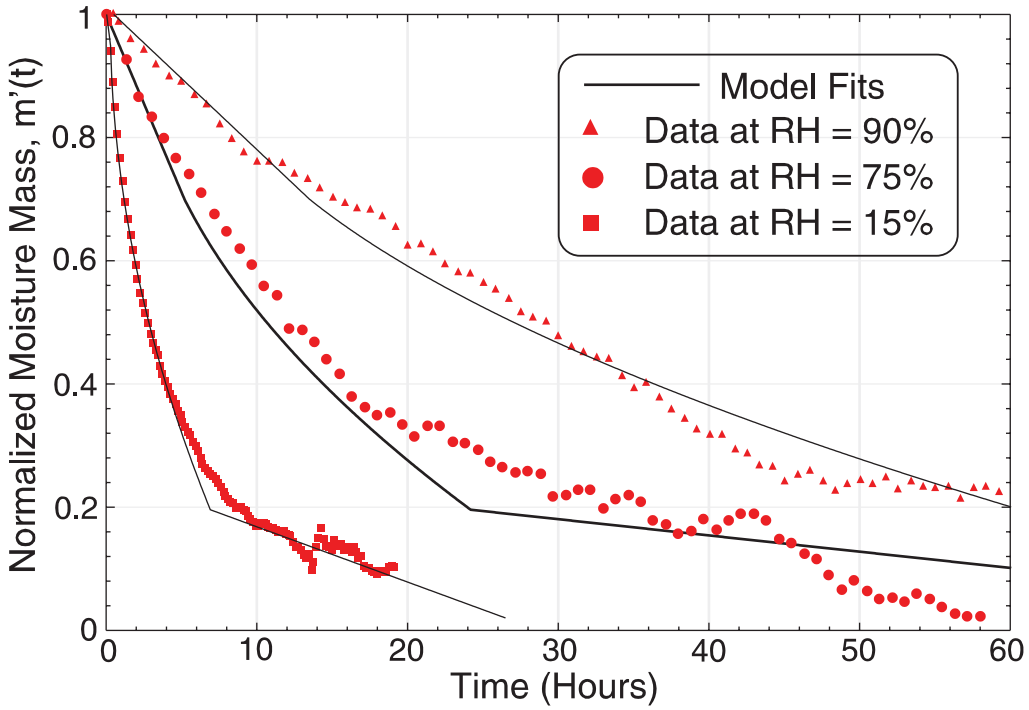

Figure 4: Drying profiles for dryer relative humidities of 15%, 75%, and 90%. The dryer temperature was 50°C, and the sample diameter and thickness were 10 cm and 1 cm, respectively. The solid lines show the drying model fits to the data.

respectively. For the sample of thickness 1 cm drying at 60°C and a relative humidity of 75%, the same average and maximum differences were 4.4% and 10.9%, respectively.

The switching point between the three stages, i.e., the value of $m'(t)$ at which the stage transition is considered to occur, depends on the drying conditions and part thickness as shown in the following logic/code block. The linear interpolations smooth the transition points.

X_1 = 0.7 ; X_2 = 0.2 ; y_1 = 0 ;

if ($L <= 0.0045$) then X_1 = 0.6;
    else if ($L <= 0.0055$) then X_1 = 0.6 + 0.1(L-0.0045)/0.001 ;

if ($RH < 0.31$) then X_1 = 0.95;
    else if ($RH < 0.4$) then X_1 = 0.95 - 0.25(RH-0.31)/0.09 ;

if ($L <= 0.003$) then X_2 = 0.05 ;
    else if ($L <= 0.01$) then X_2 = 0.05 + 0.25(L-0.003)/0.012 ;
    else if ($L > 0.015$) then X_2 = 0.3;

if ($T > 342$) then y_1 = 0.1 ;
    else if ($T > 323$) then y_1 = 0.1 + 0.1(342-T)/19 ;

if ($y_1 < X_2$ & $y_1 > 0$) then $X_2 = y_1$;

At higher drying potentials, X_1 is smaller, and X_2 is larger, compared with conditions of lower drying potential.

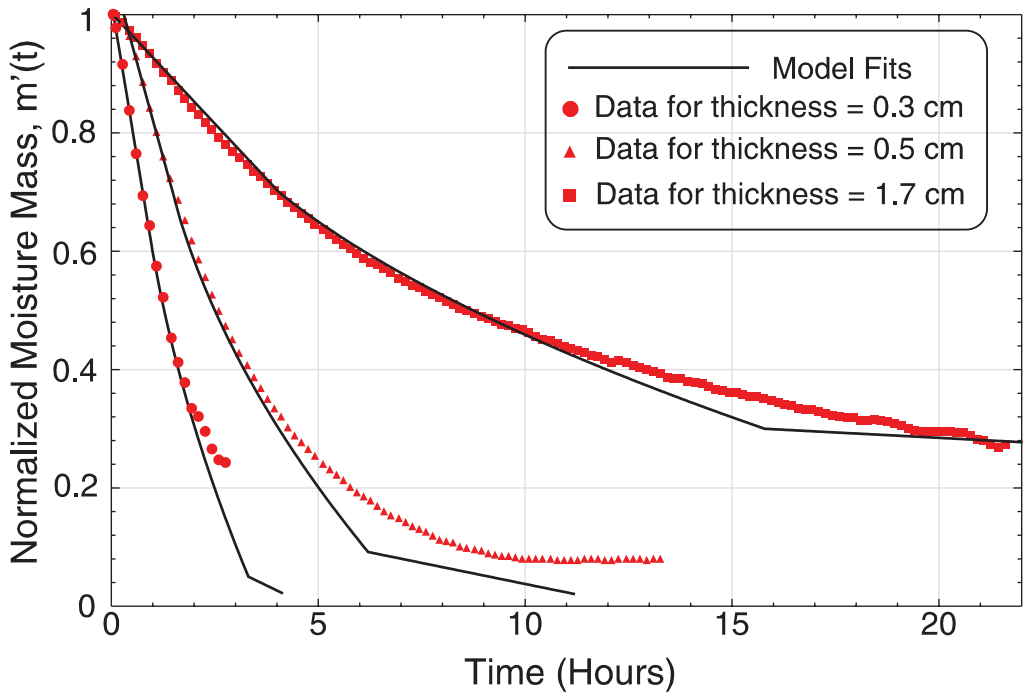

Figure 5: Drying profiles for gelcasts samples of thickness 0.3 cm, 0.5 cm, and 1.7 cm, each of diameter 10 cm. Dryer temperature and relative humidity were 50°C and 45%, respectively. The solid lines show the drying model fits to the data.

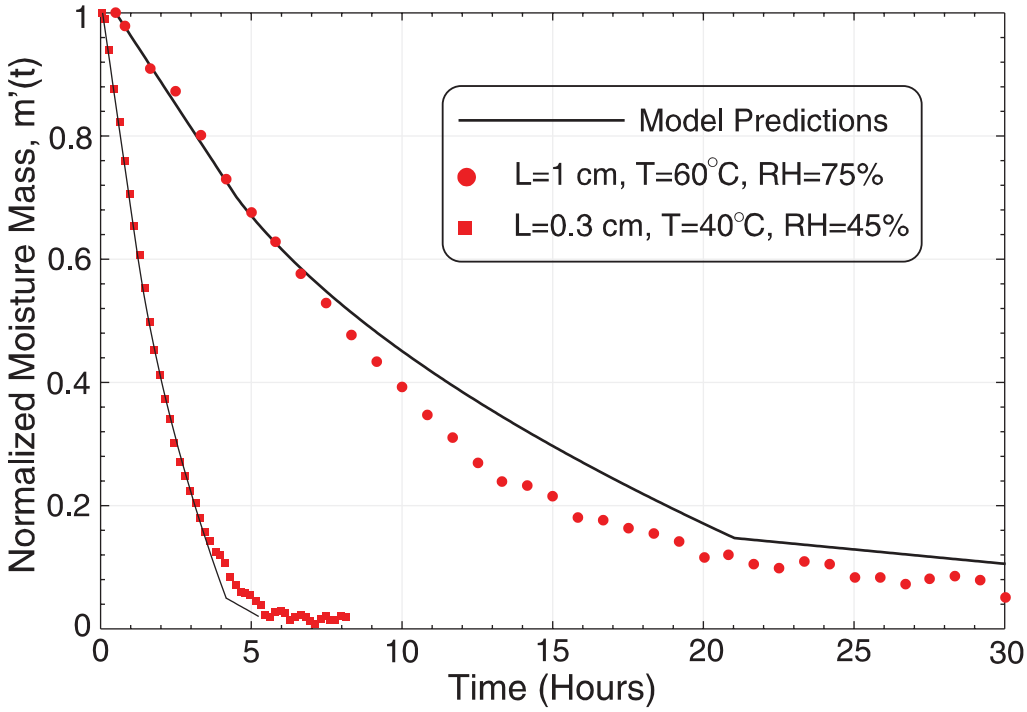

Figure 6: Cross-validation of the drying model using two gelcast samples of diameter 10 cm subject to different drying conditions. The solid lines show model predictions.

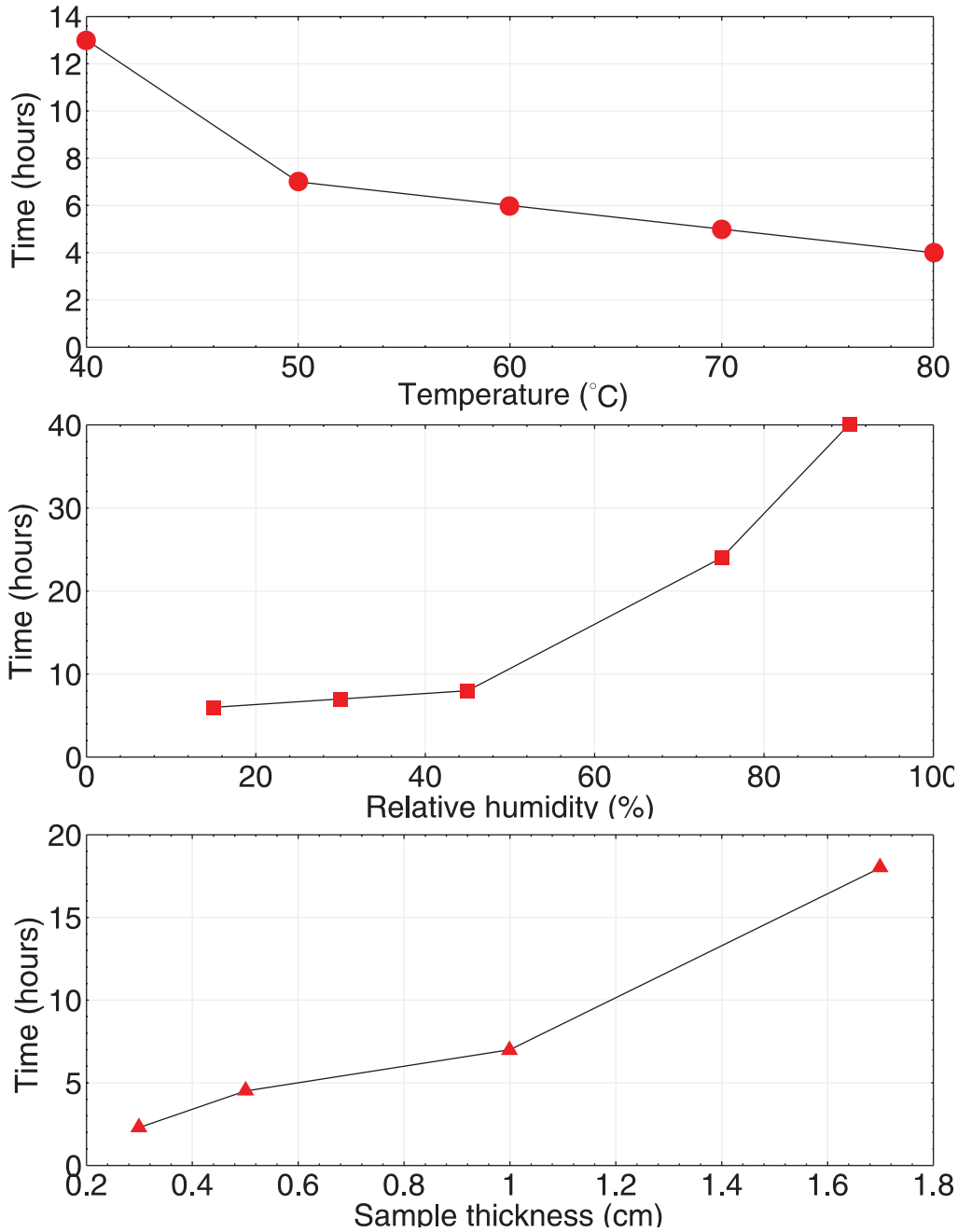

Figure 7: Time to dry 70% of the moisture in gelcast samples as functions temperature, relative humidity, and sample thickness.

Using experimental data, Figure 7 shows the time taken to achieve 70%* drying of the gelcast samples in these experiments. The graphs clearly show the non-linear dependence of drying time on each of the three variables. The drying time rises very rapidly when the dryer humidity increases above 50%.

In the experiments, the sample temperature is approximated by the sensor temperature. While the part surface may be kept at ambient (dryer) temperature, there may be temperature gradients within the sample due to evaporative

*Even the sample subjected to the lowest drying potential had at least 70% of the moisture removed in the experiments.

cooling. This temperature drop, ΔT is estimated as follows. If the drying time under high drying potential is approximately six hours (see Figure 3), then the moisture loss rate is calculated to be 1.8×10^{-6} kg/s. This evaporation rate corresponds to a latent heat loss of 4.4 W and results in cooling of the part. Heat flux then enters the sample *via* conduction from all surfaces, and in steady-state, balances the latent heat loss. The thermal conductivity, k, of the Si_3N_4 is about 7 W/m.K, but the effective thermal conductivity of the sample will be significantly smaller because of the presence of water and air pockets (of thermal conductivities of 0.5 and 0.01 W/m.K, respectively). In absence of necessary conductivity data, a conservative estimate of k of the part is 1 W/m.K. Two further assumptions are made that yield larger ΔT, *viz*, the center of the sample is at the lowest temperature, and the heat flowing into the sample from the curved surfaces is negligibly small. The conductive heat inflow rate, $\dot{q}_c$ is obtained from Fourier's law, and equals the latent heat loss of 4.4 W. Hence, we have

$$\dot{q}_c \;=\; \frac{k\,(2A)\,\Delta T}{L/2} \;=\; 4.4\,\mathrm{W}$$

For this case, ΔT is thus found to be 1.4°C. This is a negligibly small temperature drop, and the drop in typical conditions is expected to be even smaller. Thus, evaporative cooling can be neglected unless the gelcast part is several centimeters thick.

Ideally, the drying rate could be maximized at high drying potentials of high dryer temperature low humidity, thus increasing manufacturing throughput. However, rapid drying can cause stress in the parts which can lead to cracking and, hence, rejection of the cracked parts. Cracking is most likely during shrinkage when the particles are rearranging among themselves. Most of the shrinkage occurs during Stage 1 drying. Hence, it is necessary to design an optimal drying cycle whereby the drying period is minimized, but without any damage to the part.

The drying model described here was successfully used in a real-time feedback control system for optimal drying [9]. The drying recipe specified the dryer temperature and drying rate profiles. This recipe was chosen based on knowledge of critical conditions for cracking obtained from separate experiments. The controller used the model to calculate the desired dryer humidity, and to closely follow the drying trajectory specified in the recipe. Using the feedback control system, the drying time for a gelcast turbine rotor was decreased by 65% from the original open-loop process. Figure 8 shows the temperature and humidity profiles for a typical rotor drying cycle. Also shown is the dynamic sample mass, and the corresponding model prediction. The rotor was sub-divided into three parts, and the 1–D model applied to each individual part [9]. The maximum difference between the predicted dynamic mass and the actual mass measured is less than 5% for this three-dimensional drying case, with drying conditions changing over a relatively large range of temperature and relative humidity.

6 Conclusions

This paper describes a relatively simple 1–D mathematical model for the complex process of gelcast drying. While multiple physical mechanisms are involved in moisture transport, the model addresses only the rate limiting mechanisms at various stages of drying. These mechanisms are evaporation at the gelcast part surface in Stage 1 drying, water vapor diffusion through the gelcast part in Stage 2, and vapor diffusion through the dehydrated polymer network around individual gel-coated particles in Stage 3. Experimental data are used to determine certain physical parameters such as effective diffusivity of water vapor in the gelcast part, and temperature dependence of saturation vapor pressure of water associated with the gel.

This engineering model predicts drying rates for unidirectional drying with reasonable accuracy over a sufficiently broad range of part thickness, and dryer temperature and humidity. The model performed well in the context of

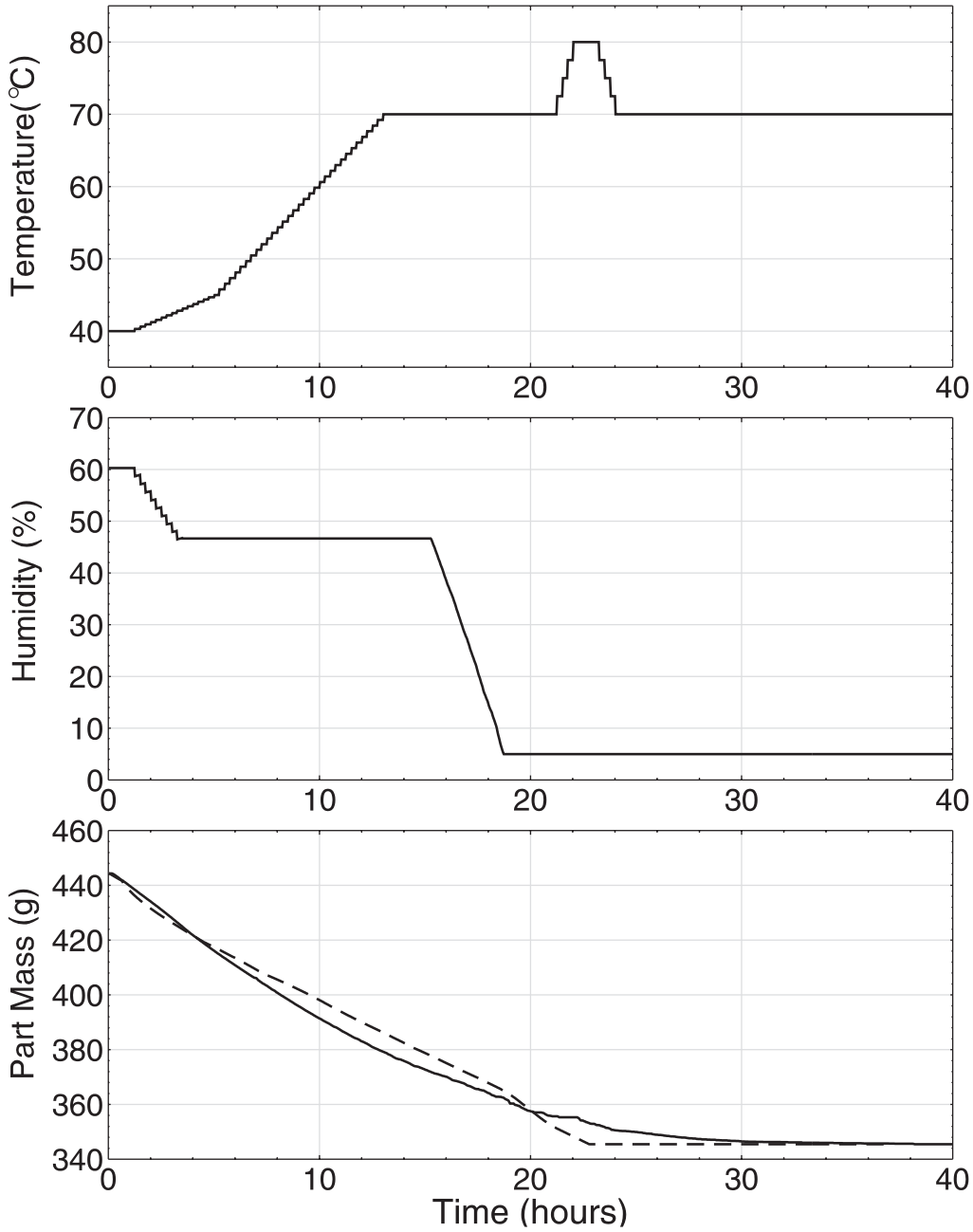

Figure 8: Dryer temperature, relative humidity, and sample mass for the drying of a rotor of an aircraft auxiliary power turbine. The dynamic sample mass measured is shown with a solid line while the model prediction weight is shown with a dashed line.

model-based control for optimal gelcast drying [9]. However, there is significant possibility of extending this work to two dimensional (axisymmetric) or three dimensional drying. Such a model could conceivably be coupled with drying stress and shrinkage models in order to present a more unified, and hence, very useful means of modeling gelcast drying. Careful experiments that measure temperatures and humidities *within* the parts during drying, as well as bulk properties such as thermal conductivity, are needed in order to use detailed models such as the one proposed by Whitaker [14].

Acknowledgement

The authors thank the reviewers for their very helpful suggestions to improve the paper. The dimension sensor used in this study was provided by L. C. Maxey of Oak Ridge National Laboratory/Lockheed Martin Energy Research, (ORNL/LMER). The authors would like to express their gratitude to Dr. O. O. Omatete and Dr. S. D. Nunn, both of ORNL, for their insight into the gelcast drying process. Dr. J. L. Ebert (SC Solutions) provided useful suggestions about the design of experiments for drying studies.

7 References

[1] O. O. Omatete, M. A. Janney, and R. A. Strehlow, "Gelcasting — A New Ceramic Forming Process", *Am. Ceram. Soc. Bull.*, **70**[10] 1641–49 (1991).

[2] A. C. Young, O. O. Omatete, M. A. Janney, and P. A. Menchhofer, "Gelcasting of Alumina", *J. Am. Ceram. Soc.*, **74**[3] 612–618 (1991).

[3] O. O. Omatete, T. N. Tiegs, and A. C. Young, "Gelcast Reaction-Bonded Silicon Nitride Composites", *Ceram. Eng. Sci. Proc.*, **12**[9–10] 2084–94 (1991).

[4] J. P. Pollinger, "Progress in Fabrication of Silicon Nitride Structural Components for Turbomachinery Applications", Presented at the International Gas Turbine And Aeroengine Congress and Exhibition , Birmingham, UK, June, 1996.

[5] C. J. Brinker and G. W. Scherer, 'Sol-Gel Science', pp. 407–513, Academic Press, 1990.

[6] G. W. Scherer, "Theory of Drying", *J. Am. Ceram. Soc.*, **73** [1] 3–14 (1990).

[7] J. S. Reed, 'Introduction to the Principles of Ceramic Processing', pp. 411–424, John Wiley and Sons, 1995.

[8] O. O. Omatete, R. A. Strehlow, and C. A. Walls, "Drying of Gelcast Ceramics", *Trans. Am. Ceram. Soc.*, **26** 101–107 (1992).

[9] Y. P. Harn, S. Ghosal, G. Aral, A. Emami-Naeini, B. Draskovich, and L. C. Maxey, 'Real-Time Model-Based Control Systems Design for Gelcast Drying Process', Proceedings of the 1997 IEEE International Conference on Control Applications, Hartford, CT., pp. 271–276, Oct. 5–7, IEEE, 1997.

[10] F. A. L. Dullen, 'Porous Media, Fluid Transport, and Pore Structure', pp. 387–395, Academic Press, 1992.

[11] J. P. Holman, 'Heat Transfer', McGraw Hill, 5^{th} Edition, 1981.

[12] E. L. Cussler, 'Diffusion Mass Transfer in Fluid Systems', Cambridge University Press, 1984.

[13] R. B. Bird, W. E. Stewart, and E. N. Lightfoot, 'Transport Phenomena', pp. 505, John Wiley and Sons, 1960.

[14] S. Whitaker, in 'Advances in Drying', Vol. I, ed. A. S. Mujumdar, pp. 23–61, Hemisphere, New York, 1980.